Available online at www.sciencedirect.com
ScienceDirect
International Journal of Heat and Fluid Flow 28 (2007) 496–511
International Journal of HEAT AND FLUID FLOW
www.elsevier.com/locate/ijhff

Buoyancy suppression in gases at high temperatures

Maria A. Kuczmarski *, Suleyman A. Gokoglu

NASA Glenn Research Center, 21000 Brookpark Road, Cleveland, OH 44135, United States

Received 18 December 2005; received in revised form 23 May 2006; accepted 3 July 2006
Available online 25 September 2006

Abstract

The computational fluid dynamics code FLUENT was used to study Rayleigh instability at large temperature differences in a sealed gas-filled enclosure with a cold top wall and a heated bottom wall (Bénard problem). Both steady state and transient calculations were performed. Instability boundaries depending on the geometry, temperature, and pressure were defined that showed the system tended to become more unstable when the hot-wall temperature increased beyond a certain level, a result of the dampening effect of gas viscosity at higher temperatures. Results also showed that the eventual system stability depended on the final pressure reached at steady state, regardless of how fast the bottom-wall temperature was ramped up to minimize time spent in the unstable region of fluid motion. It was shown that the final system state can differ depending on whether results are obtained via a steady-state or transient calculation, demonstrating that the history of the flow structure development and corresponding temperature fields in this type of system has a profound effect on the final state. Finally, changes in the slope of the pressure-versus-time curve were found to be good indicators of flow pattern changes, and can be a convenient experimental tool for diagnosing the expected changes in flow behavior in such systems.

Keywords: Buoyancy; Natural convection; Numerical modeling; Bénard problem

1. Introduction

When a horizontal enclosed space is heated to a uniform bottom-wall temperature greater than that of the top wall, an upwardly decreasing temperature profile is established. For a sufficiently small temperature difference between the bottom and top walls, viscous forces are greater than buoyancy forces, and the fluid remains quiescent. However, as this temperature difference increases, a point will be reached at which the buoyancy forces will become greater than the viscous forces, and the fluid begins to move. This is known as the classic Bénard problem.

The Rayleigh number is used to define the onset and development of buoyant flow under these conditions. It is defined as

$$Ra \equiv \frac{(\rho_i - \rho)}{\rho_i} \frac{gL^3}{\alpha \nu} \tag{1}$$

where

$$\nu = \frac{\mu}{\rho} \tag{2}$$

$$\alpha = \frac{k}{\rho C_P} \tag{3}$$

The Rayleigh number can also be expressed as the product of the Grashof number, Gr, and the Prandtl number, Pr,

$$Ra = Gr \times Pr \tag{4}$$

where

$$Gr \equiv \frac{(\rho_i - \rho)}{\rho_i} \frac{gL^3}{\nu^2} \tag{5}$$

and

$$Pr \equiv \frac{\nu}{\alpha} = \frac{\mu C_P}{k} \tag{6}$$

* Corresponding author. Tel.: +1 216 433 3651; fax: +1 216 433 5033.
E-mail address: Maria.A.Kuczmarski@nasa.gov (M.A. Kuczmarski).

0142-727X/$ - see front matter © 2006 Elsevier Inc. All rights reserved.
doi:10.1016/j.ijheatfluidflow.2006.07.006

Nomenclature

C_p	heat capacity at constant pressure (kJ/kg K)
g	gravitational constant (m/s^2)
Gr	Grashof number (dimensionless)
Gr_0	Grashof number evaluated at cold-wall temperature (dimensionless)
k	thermal conductivity (W/m K)
L	characteristic length (m)
P	pressure (atm)
P_i	initial pressure (atm)
P_f	final pressure (atm)
Pr	Prandtl number (dimensionless)
Q	total heat transfer rate (J/s)
Ra	Rayleigh number (dimensionless)
Ra_c	critical Rayleigh number (dimensionless)
T	temperature (K)
T_*	arithmetic mean temperature (K)
T_c	cold-wall temperature (K)
T_h	hot-wall temperature (K)
T_i	initial temperature (K)
V_{max}	maximum velocity (m/s)

Greek symbols

α	thermal diffusivity (m^2/s)
β_T	coefficient of thermal expansion at constant pressure (K^{-1})
μ	dynamic viscosity (kg/m s)
ν	kinematic viscosity (m^2/s)
ν_0	kinematic viscosity evaluated at cold-wall temperature (m^2/s)
ρ	density (kg/m^3)
ρ_i	initial density (kg/m^3)

The fluid remains stable if the Rayleigh number is less than the critical Rayleigh number, Ra_c. Once the critical Rayleigh number is exceeded, finger-like intrusions of the lighter gas into the heavier gas and the heavier gas into the lighter gas result. Goldstein and Volino (1995) have presented a summary of various investigations in the literature for the onset of convection and flow development in horizontal layers. Widely ranging values of the critical Rayleigh number were reported, anywhere from 1000 to 3000.

While the above studies used different criteria and different experimental observations as the basis for determining the onset of instability, one possible explanation for this wide range of values is that the Rayleigh and Grashof numbers are derived assuming the Boussinesq approximation. This assumes that all fluid properties are constant, except for density in the buoyancy term of the momentum equation, and that viscous dissipation can be neglected (Kays and Crawford, 1980). Under these conditions, the density difference can be approximated as

$$\frac{(\rho_i - \rho)}{\rho_i} = \beta_T (T - T_i) \tag{7}$$

where

$$\beta_T = -\left(\frac{1}{\rho}\right) \times \left(\frac{\partial \rho}{\partial T}\right)_P \tag{8}$$

β_T is the coefficient of thermal expansion at constant pressure.

The temperature dependence of thermodynamic and transport properties can often be safely neglected at small temperature differences. Under non-Boussinesq conditions, the predictive abilities of dimensionless numbers derived by assuming Boussinesq conditions require more attention. Gray and Giorgini (1976) and Paolucci and Chenoweth (1987) reported on the validity of the Boussinesq approximation and departures from it. These studies led to the specification of conditions under which it is justified to neglect certain terms in the Boussinesq approximation.

Under non-Boussinesq conditions (large normalized temperature differences), the temperature dependence of thermodynamics and transport properties becomes important and their effects must be included in order to obtain accurate descriptions of the state of flow inside the enclosure. Frolich et al. (1992) studied large departures from the Boussinesq approximation in the Rayleigh–Bénard problem. They found that temperature-dependent properties affected the mid-plane symmetry and led to both quantitative and qualitative changes in the flow, particularly in the bifurcation from the conduction state. They found that the non-Boussinesq behavior became confined to small regions in the flow, and concluded that the relative importance of these effects would, therefore, diminish for higher Rayleigh numbers. This conclusion, however, fails to consider that gases tend to become more stable at large normalized temperature differences due to the dampening effect of gas viscosity at high temperatures, an effect investigated in this paper.

We limit ourselves here to consideration of gaseous media only. For ideal gases, it can be readily shown that

$$\beta_T = \frac{1}{T} \tag{9}$$

Using Eqs. (1), (5), (7), and (9), the Rayleigh and Grashof numbers can now be expressed as

$$Ra = \frac{\beta_T \Delta T g L^3}{\nu \alpha} \tag{10}$$

$$Gr = \frac{\beta_T \Delta T g L^3}{\nu^2} \tag{11}$$

The power-law approximations of the temperature dependence of other gaseous properties are typically taken as (Svehla, 1962)

$$\rho \propto T^{-1} \tag{12}$$

$$\mu \propto T^{0.7} \tag{13}$$

$$k \propto T^{0.85} \tag{14}$$

$$C_P \propto T^{0.19} \tag{15}$$

$$D \propto T^{1.7} \tag{16}$$

These powers are consistent with the kinetic theory of gases (Kennard, 1938; Hirschfelder et al., 1954), and accurate descriptions for the properties of air in the 600–1600 K range (Brown and Donoughe, 1951; Kays and Crawford, 1980).

Based on the temperature dependencies given in Eqs. (12)–(16), we can determine the temperature dependence of the dimensionless numbers describing the relative importance of momentum, heat, and species mass diffusion, the Prandtl (Pr), Schmidt (Sc), and Lewis (Le) numbers:

$$Pr \equiv \frac{\nu}{\alpha} = \frac{C_P \mu}{k} \propto T^{0.04} \tag{17}$$

$$Sc \equiv \frac{\nu}{D} = \frac{\mu}{\rho D} \propto T^{0} \tag{18}$$

$$Le \equiv \frac{\alpha}{D} = \frac{k}{\rho C_P D} \propto T^{-0.04} \tag{19}$$

Since these numbers are relatively temperature independent, ignoring the variable property effects is justified by many convection problems.

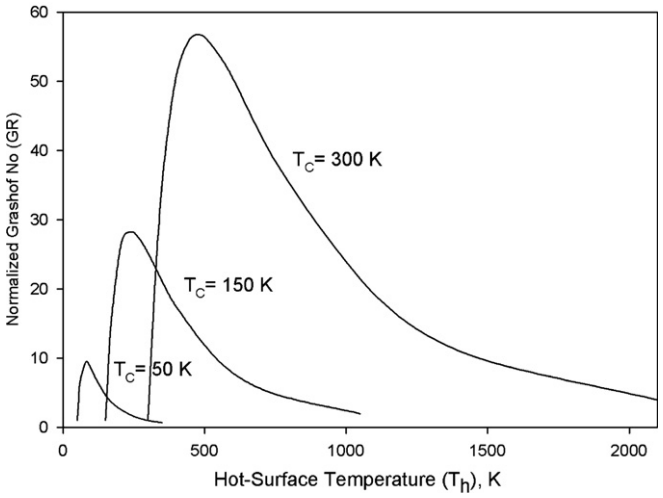

Fig. 1. Variation of normalized Grashof number with hot-wall temperature (Eq. (25)) describing the effect of temperature-dependent gas properties.

Table 1
Grid sensitivity study results

Grid	# Cells in X	# Cells in Y	% Change in Q (J/s)
Grid0	60	10	
Grid1	120	20	$(Q1–Q0)/Q0 = 0.03$
Grid2	240	40	$(Q2–Q1)/Q1 = 0.009$
Grid3	480	80	$(Q3–Q2)/Q2 = 0.002$

For large normalized temperature differences, the temperature-dependent gas properties are typically accounted for by evaluating their values at a reference temperature.

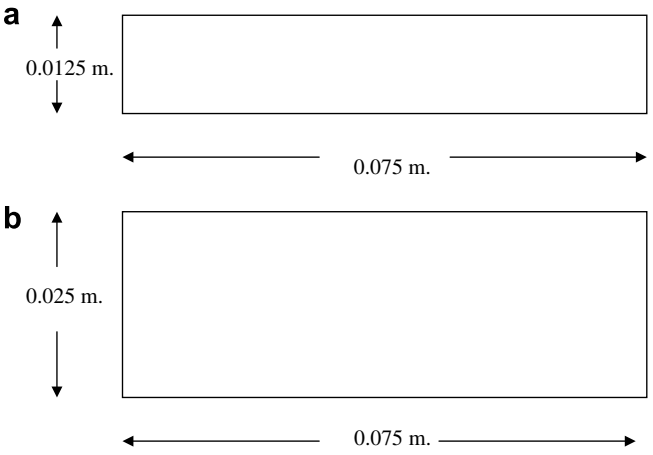

Fig. 2. Diagrams of configurations modeled for this paper. (a) case 1, (b) case 2, which is the same in length as case 1, but double the height.

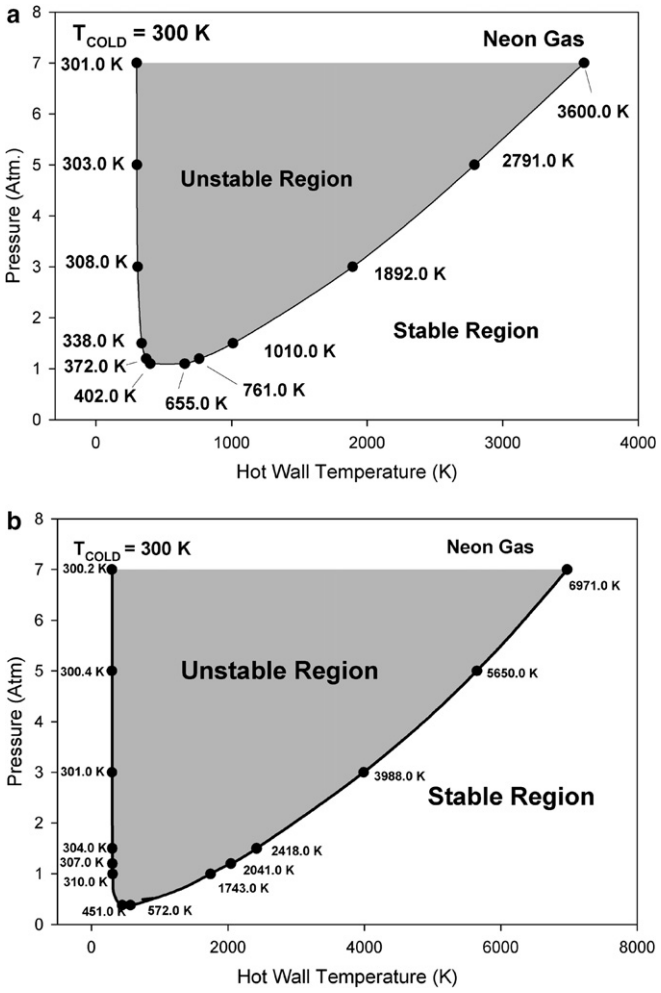

Fig. 3. A schematic of calculated stable and unstable regions for neon for (a) case 1, (b) case 2. Hot surface temperatures at which transition occurs at various pressures are indicated.

This is usually taken to be the arithmetic mean of the hot and cold-wall temperatures in the system (Kays and Crawford, 1980; Bird et al., 1960):

$$T_* = T_c + 0.5(T_h - T_c) = \frac{(T_h + T_c)}{2} \tag{20}$$

Paolucci and Chenoweth (1987) found in their calculations that this reference temperature describes average properties more accurately than other alternatives.

Using Eqs. (9), (10), (12)–(15), the temperature dependence of the Raleigh number can now be expressed as

$$Ra \propto \Delta T T_*^{-4.36} \tag{21}$$

Using Eqs. (9), (11)–(13), the temperature dependence of the Grashof number can now be expressed as

$$Gr \propto \Delta T T_*^{-4.40} \tag{22}$$

Since the temperature dependencies of the Rayleigh and Grashof numbers become about the same, we focus our attention to Gr from now on. It is interesting to note that the temperature dependence of ν, the gas kinematic viscosity, is primarily responsible for making the Grashof number so strongly temperature dependent.

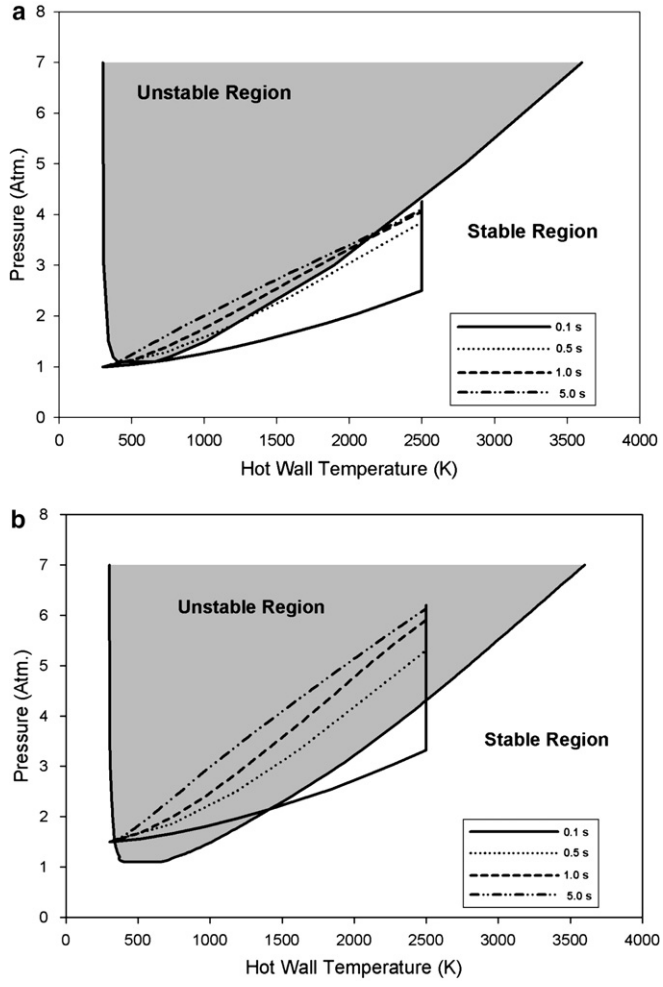

Fig. 4. Case 1: pressure vs. hot-wall temperature for various hot-wall temperature ramp times, (a) $P_i = 1.0$ atm, (b) $P_i = 1.5$ atm.

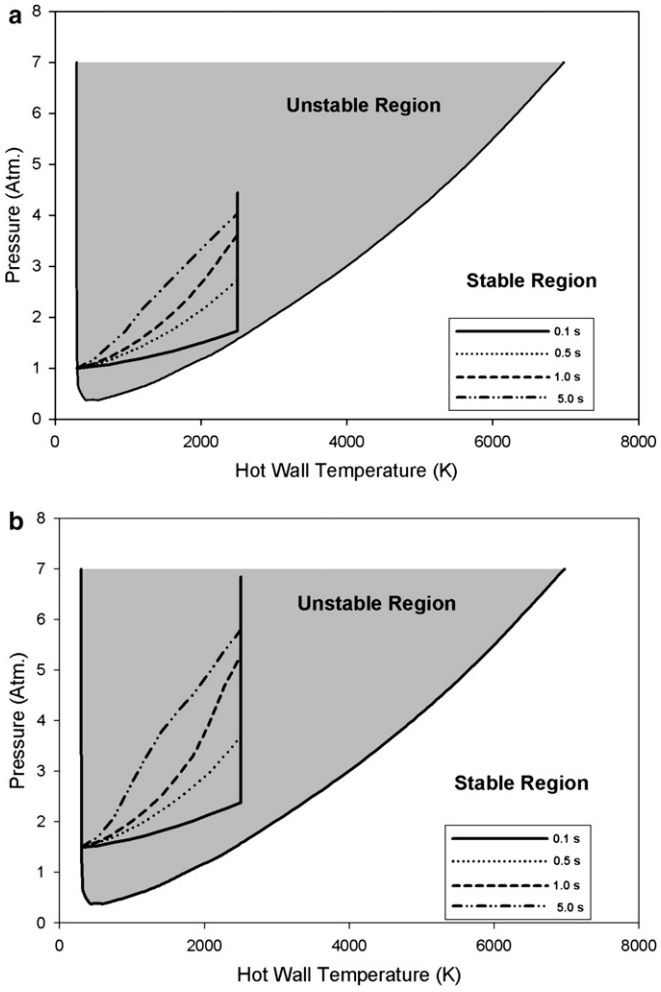

Fig. 5. Case 2: pressure vs. hot-wall temperature for various hot-wall temperature ramp times, (a) $P_i = 1.0$ atm, (b) $P_i = 1.5$ atm.

Table 2
Comparison of final predicted by the ideal gas law and FLUENT

Case	P_i (atm)	Ramp time (s)	P_f (atm) ideal gas law	P_f (atm) FLUENT	% Difference
1	1.0	0.1	4.67	4.27	−8.6
1	1.0	0.5	4.67	4.27	−8.6
1	1.0	1.0	4.67	4.17	−10.7
1	1.0	5.0	4.67	4.17	−10.7
1	1.5	0.1	7.0	6.20	−11.4
1	1.5	0.5	7.0	6.19	−11.6
1	1.5	1.0	7.0	6.19	−11.6
1	1.5	5.0	7.0	6.19	−11.6
2	1.0	0.1	4.67	4.45	−4.7
2	1.0	0.5	4.67	4.45	−4.7
2	1.0	1.0	4.67	3.99	−14.6
2	1.0	5.0	4.67	4.13	−11.6
2	1.5	0.1	7.0	6.81	−2.7
2	1.5	0.5	7.0	6.81	−2.7
2	1.5	1.0	7.0	6.81	−2.7
2	1.5	5.0	7.0	6.23	−11.0

The Boussinesq approximation is typically valid if:

$$\frac{\Delta T}{T_*} \leqslant 0.1 \tag{23}$$

When T_c is room temperature around 300 K, ΔT must be smaller than about 35 K. For most heat transfer applications, ΔT is much larger than this. For combustion applications, it routinely exceeds 1000 K. Hence, care must be taken in using the Rayleigh stability criteria or heat transfer correlations based on the Rayleigh or Grashof numbers.

For quantifying the temperature dependence of the Grashof number, consider a constant property Grashof number, Gr_0, for which the gas properties are evaluated at the cold-wall temperature T_c, and the normalized temperature difference is taken as unity (or $\Delta T = 1$ K):

$$Gr_0 = \frac{1}{T}\frac{gL^3}{v_0^2} \tag{24}$$

Then the variation of the Grashof number with temperature at larger normalized temperature differences can be quantified by normalizing the Grashof number with respect to Gr_0. The normalized Grashof number, defined as GR, then has the following temperature dependence:

$$GR \equiv \frac{Gr}{Gr_0} = \Delta T\left(\frac{T_c}{T_*}\right)^{4.4} \tag{25}$$

Note that Eq. (25) is independent of the type of gas and the pressure of the system as long as the power-law descriptions for the temperature dependence of gas properties are adequate. Fig. 1 describes the behavior of GR for three different cold-wall temperatures. The curve for the cold-wall temperature of $T_c = 300$ K forms the basis of most of the discussions presented in this paper. Curves for lower cold-wall temperatures apply to arguments related to cryogenic applications.

Fig. 1 has a number of interesting implications. It suggests that if a system becomes unstable when the hot-wall temperature is increased, then there are two distinct critical hot-wall temperatures for the onset of buoyant convection, one at the lower temperature and another at a higher temperature. Below and above these temperatures, the system

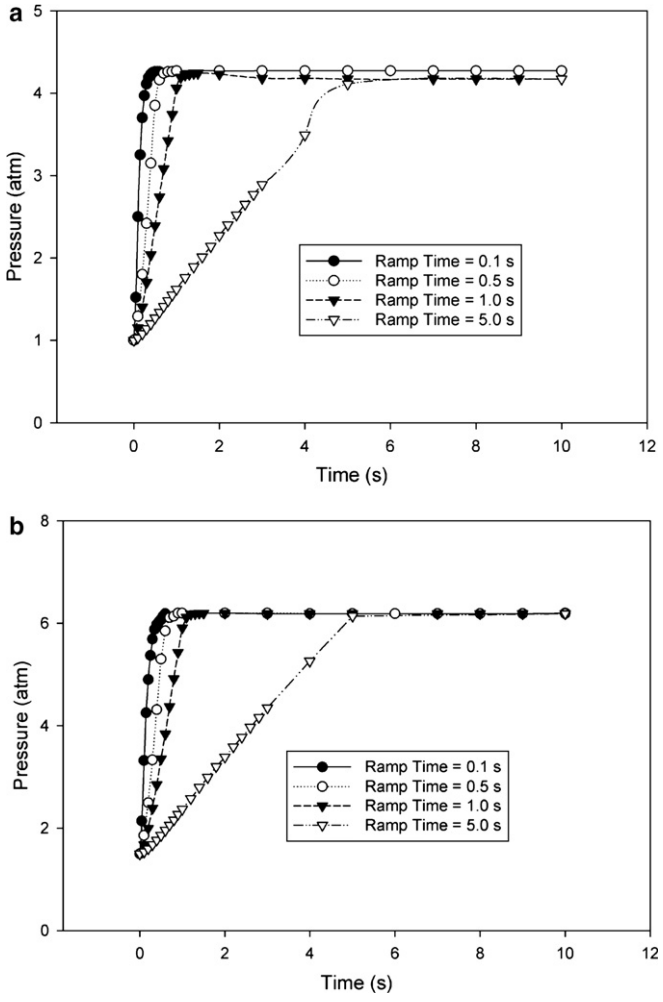

Fig. 6. Case 1: pressure vs. time for various hot-wall temperature ramp times, (a) $P_i = 1.0$ atm, (b) $P_i = 1.5$ atm. Note the different scales on the two plots.

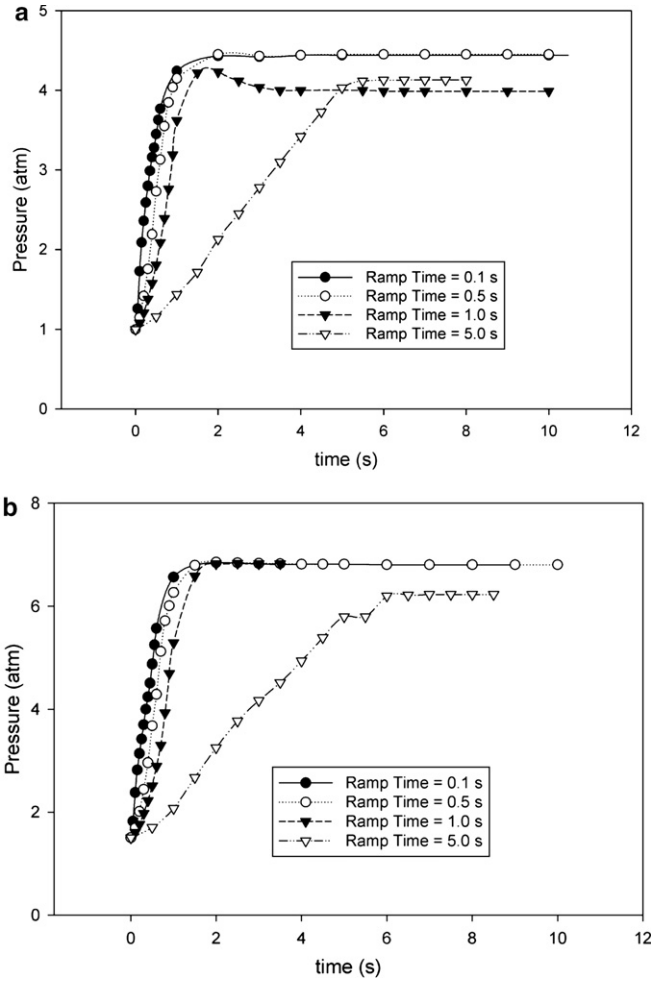

Fig. 7. Case 2: pressure vs. time for various hot-wall temperature ramp times, (a) $P_i = 1.0$ atm, (b) $P_i = 1.5$ atm. Note the different scales on the two plots.

is stable, i.e., conduction-dominated. It seems that, for a fixed cold-wall temperature, the lower the critical low-temperature is for a system, the higher the critical high-temperature is. The question of whether there is any significant difference in the critical Rayleigh numbers for the onset of convection at the lower and higher temperature regions will be explored below.

In a previous paper, Gokoglu and Kuczmarski (2003) showed via a steady state analysis that for temperature differences larger than justifiable for the Boussinesq approximation, there are situations were a gaseous system will never experience the onset of buoyant convection, no matter how large the temperature difference becomes at a given pressure. This was due to the temperature-dependent gas properties, particularly that of the kinematic viscosity, which tended to counteract the tendency toward instability at higher temperatures. In addition, two critical hot-wall temperatures were shown to exist for a given pressure, above and below which the system was stable.

In this paper, transient calculations have been performed to examine the behavior of the system as it pressurizes while the bottom wall is heated at different rates. These transient solutions are carried out over a sufficiently long time period to allow comparison between results obtained from transient solutions and those obtained using steady-state solutions at the final prevailing pressure. The development of the flow field over time for different heating rates and its effect on the temperature field is demonstrated. In addition, the effect of varying the enclosure height on the predicted range of instability is examined.

2. Numerical models

This investigation used the computational fluid dynamics code FLUENT (Fluent, Inc.), which uses a finite volume method to discretize the continuity, momentum, and energy equations. Two 2-D models of a rectangular geometry were constructed, as shown in Fig. 1. Case 2 has a distance between the hot and cold walls that is twice that of case 1. Adiabatic boundary conditions were set along both side walls, and the top cold-wall temperature was set at 300 K. The bottom hot-wall temperature was set at 2500 K for the steady-state cases, or ramped to a final temperature of 2500 K for the transient cases. Neon gas was

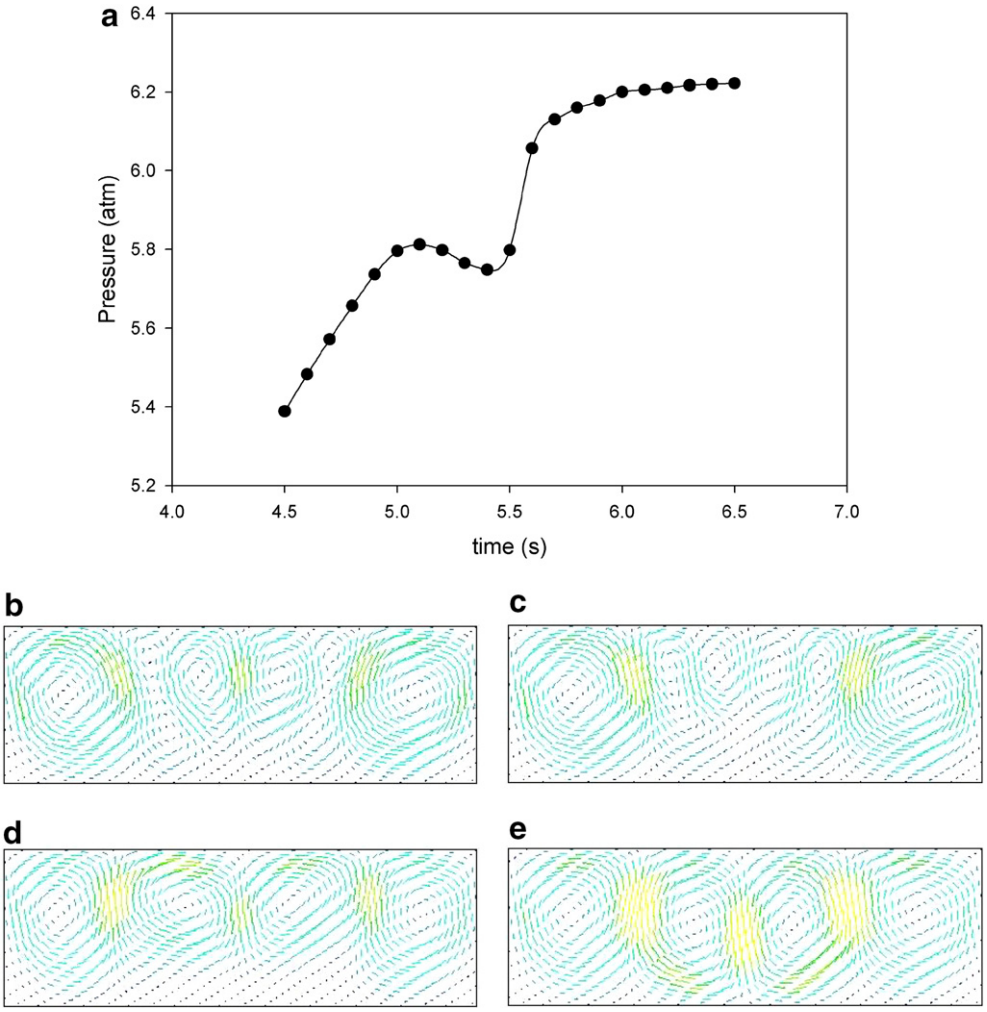

Fig. 8. Case 2: (a) pressure vs. time for the 5 s temperature ramp between 4.5 and 6.5 s; velocity fields at: (b) 5.0 s, (c) 5.2 s, (d) 5.4 s, (e) 5.6 s.

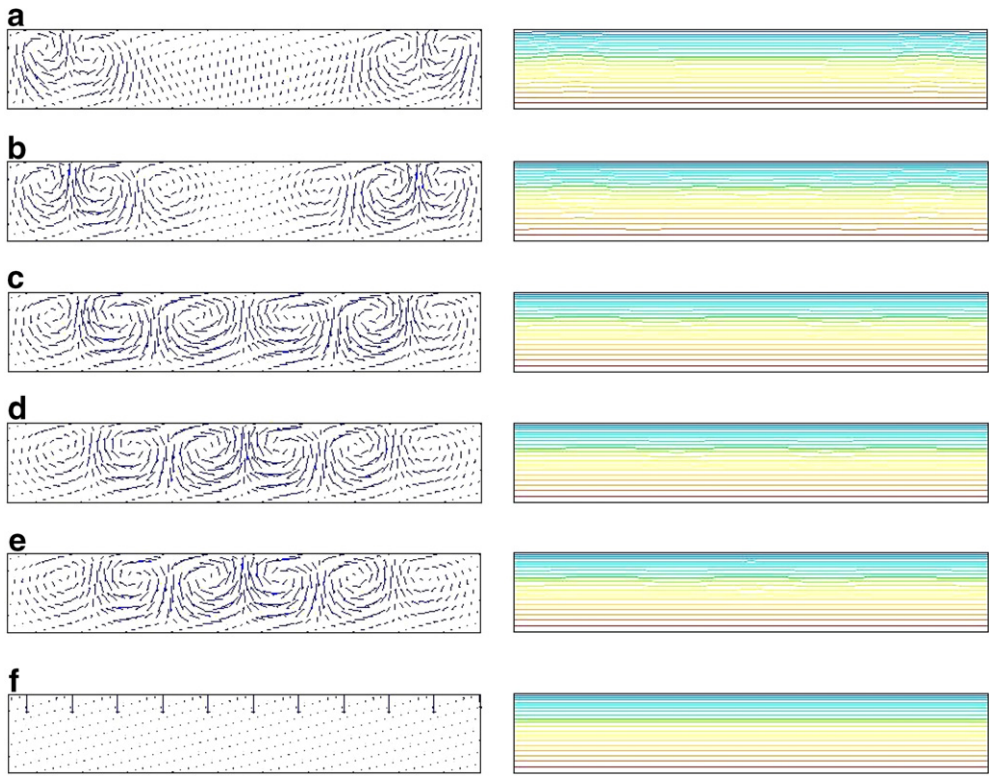

Fig. 9. Velocity and temperature fields in neon, case 1. Final $T_h = 2500$ K, $P_i = 1.0$ atm. Transient solution with a 0.1 s bottom wall temperature ramp after: (a) 0.3 s ($V_{max} = 0.007$ m/s), (b) 0.5 s ($V_{max} = 0.004$ m/s), (c) 2.0 s ($V_{max} = 0.0007$ m/s), (d) 5.0 s ($V_{max} = 0.0006$ m/s), (e) 10.0 s ($V_{max} = 0.0006$ m/s); (f) steady-state solution ($V_{max} = 0.009$ m/s). 0.5 s temperature ramp yields similar results.

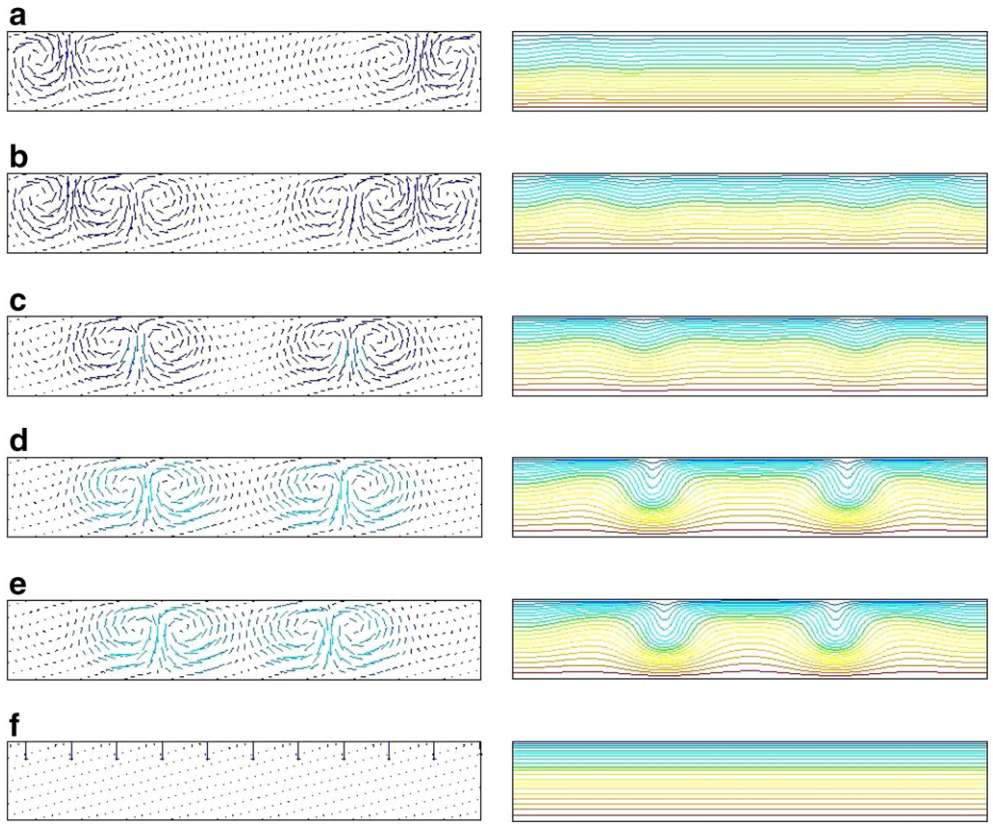

Fig. 10. Velocity and temperature fields in neon, case 1. Final $T_h = 2500$ K, $P_i = 1.0$ atm. Transient solution with a 1.0 s bottom wall temperature ramp after: (a) 0.5 s ($V_{max} = 0.01$ m/s), (b) 0.8 s ($V_{max} = 0.02$ m/s), (c) 1.5 s ($V_{max} = 0.04$ m/s), (d) 5.0 s ($V_{max} = 0.1$ m/s), (e) 10.0 s ($V_{max} = 0.1$ m/s); (f) steady-state solution ($V_{max} = 0.009$ m/s). 5.0 s temperature ramp yields similar results.

used in the enclosure. For the steady-state cases, the operating pressure was defined, along with a hot-wall temperature of 2500 K. The standard discretization scheme in FLUENT was used for pressure and the SIMPLE algorithm for the pressure–velocity coupling (Caretto et al., 1972; FLUENT User's Guide, 2005). A second order upwind scheme was used for the continuity, momentum, and energy equations. For the transient calculations, an initial pressure was specified, but a floating operating pressure was defined in the model to allow the pressure to increase as the gas was heated. A second order upwind scheme was used for the momentum and energy equations, and for the density interpolation scheme. The PRESTO! discretization scheme was used for pressure (Patankar, 1980, FLUENT User's Guide), and the PISO algorithm was employed for the pressure–velocity coupling (Issa, 1986; Ferzieger and Peric, 1996, FLUENT User's Guide). A second order upwind scheme was used for the continuity, momentum, and energy equations. A time step of 1×10^{-4} s was used for all transient calculations. Larger time steps led to problems with convergence. The underrelaxation factors were set to 1 for pressure, density, body forces, momentum, and energy. This helped speed the computations that were slowed by the necessity of choosing a small time step. The solutions were considered converged for steady-state solutions when the scaled residuals dropped below 1×10^{-3} for the continuity equation, 1×10^{-5} for the momentum equations, and 1×10^{-6} for the energy equation. Convergence for the transient solutions required these values to be obtained for each time step. All transient cases were run up to ten seconds.

Four different grid densities were examined for case 1 to study the solution grid sensitivity. The total heat transfer rate at the heated bottom wall was compared among the four grids, since this heat transfer into the system was the ultimate source for all changes experienced by the system. Table 1 shows the number of computational cells used for each grid, along with the total heat transfer rate at the bottom wall, Q, and the change in this rate between consecutive grids. The change in the total heat transfer rate is of the same order of magnitude between grids 1 and 2 as it is between grids 2 and 3; both are at very small values. Because the computational time increases with the grid density, grid 2 was chosen to balance higher resolution with reasonable run times. All results in the rest of this paper for case 1 were obtained using grid 2.

For case 2, the grid used was based on grid 2 discussed above. The number of computational cells in the X-direction remained the same at 240 cells, but the number of computational cells in the Y-direction was simply doubled from 40 cells to 80 cells since the height of case 2 is double that of case 1 (see Fig. 2).

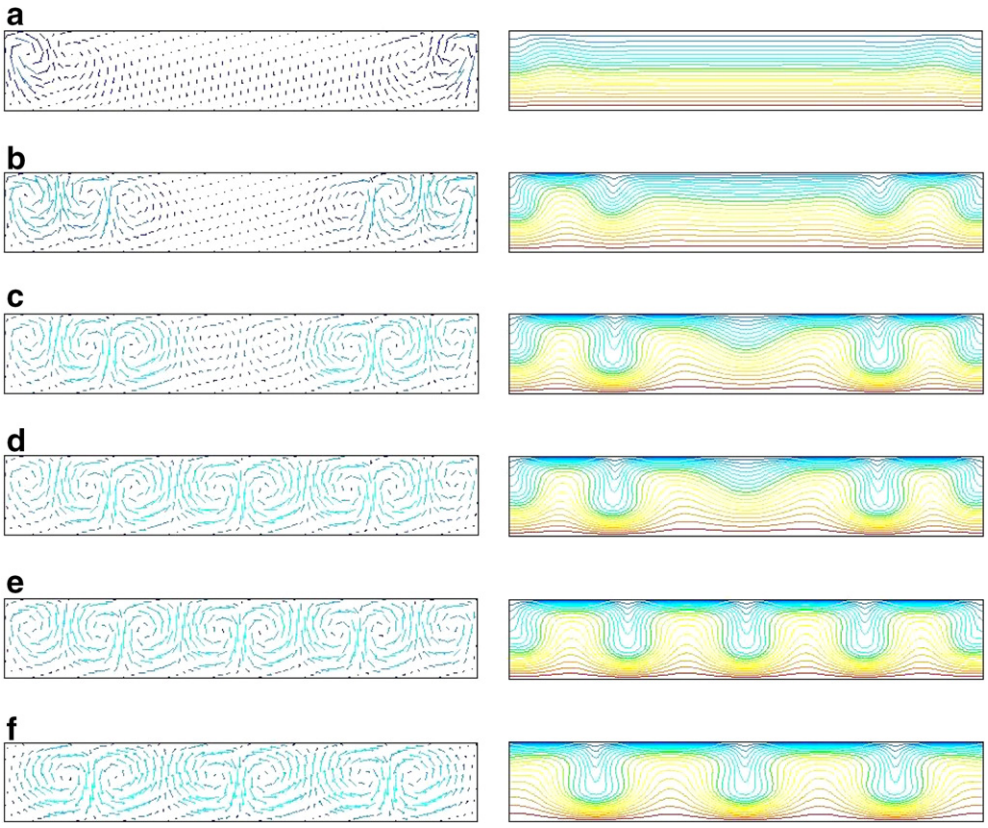

Fig. 11. Velocity and temperature fields in neon, case 1. Final $T_h = 2500$ K, $P_i = 1.5$ atm. Transient solution with a 0.1 s bottom wall temperature ramp after: (a) 0.2 s ($V_{max} = 0.03$ m/s), (b) 0.4 s ($V_{max} = 0.09$ m/s), (c) 0.6 s ($V_{max} = 0.2$ m/s), (d) 0.8 s ($V_{max} = 0.2$ m/s), (e) 10.0 s ($V_{max} = 0.2$ m/s); (f) steady-state solution ($V_{max} = 0.2$ m/s). 0.5 and 1.0 s temperature ramps yield similar results.

3. Results and discussion

First, the upper and lower temperature limits on stability were determined for the two cases with different enclosure heights by running steady-state cases at various pressure levels. The results are shown in Fig. 3. It can be seen that regardless of the temperature difference, some systems always remain stable below a certain minimum pressure, depending on the height of the geometry. Neon was stable for all hot-wall temperatures at 1 atm of pressure or less for case 1, but the pressure needed to be decreased to 0.36 atm or less in case 2 before neon was stable at all hot-wall temperatures. In addition, the range of pressures and temperatures for which the system is unstable is expectedly much greater for case 2 than for case 1 since the characteristic length, i.e., the height between the top and bottom walls in this study, is doubled in case 2, resulting in an eight-fold increase in the Rayleigh number. These results also confirm the original findings of Gokoglu and Kuczmarski (2003) that the tendency of a system to become more unstable can actually decrease when hot-wall temperature is increased beyond a certain level where the dampening effect of gas viscosity becomes more prevalent.

Next, transient runs were conducted to examine the behavior of the system as it dynamically develops. The same scales were used for Figs. 9–18, i.e., a range of 2×10^{-8} to 5×10^{-1} m/s for velocity and a range of 300–2500 K for temperature. The curves showing the rise in pressure with the bottom-wall temperature are plotted in Figs. 4 and 5 for both cases at initial pressures of 1.0 and 1.5 atm. The bottom-wall temperature was ramped to a final temperature of 2500 K over 0.1, 0.5, 1.0, and 5.0 s. The curves are superimposed over the results obtained from steady-state calculations showing the stable and unstable regions. For all ramp times, the system crosses over into the unstable region at least part of the time. For case 1, at an initial pressure of 1 atm, all cases cross back over to the stable region at the end of the ramp, although they remain very close to the transition line. For case 2, at an initial pressure of 1 atm, the system quickly crosses into the unstable region and remains there for the 0.5, 1.0, and 5.0 s ramp times. For the 0.1 s ramp time, the curve crosses over into the stable region again, but after the final hot-wall temperature is reached, the pressure continues to rise towards its steady state, and the system ends up back in the unstable region. So, even though the bottom-wall temperature can be ramped at a rate that causes the system to undergo a stable–unstable–stable transition, the system will eventually end up in a region defined by the final pressure the system rises to. This pressure can be estimated using the ideal gas law:

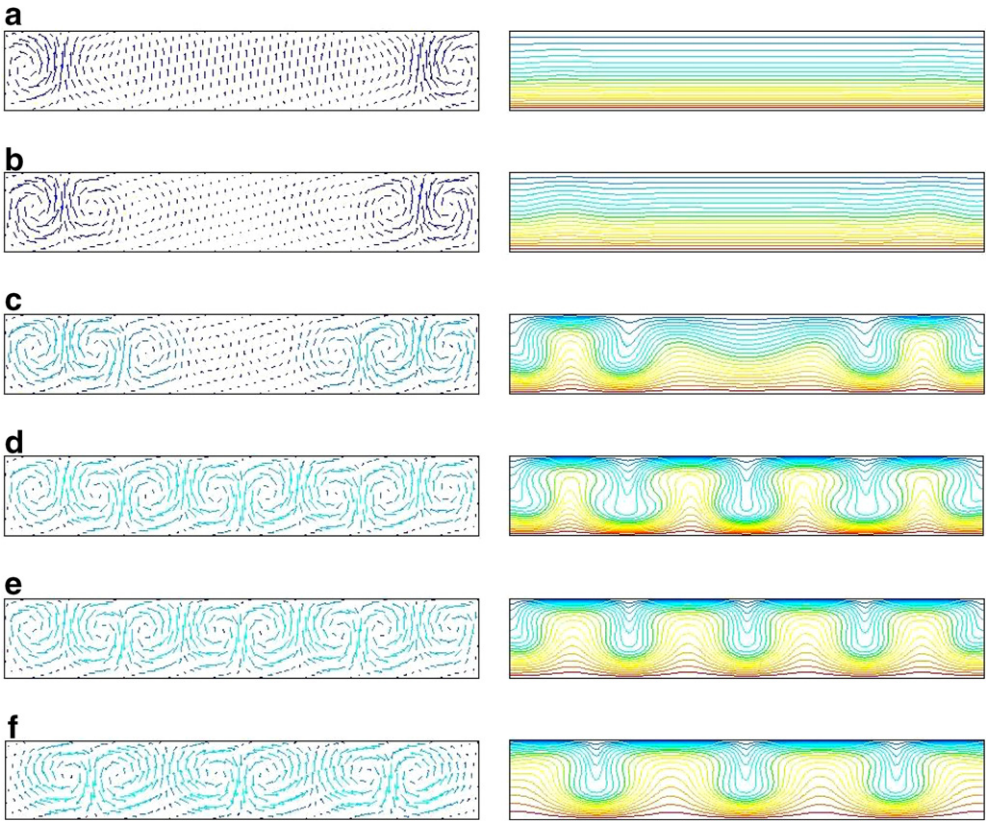

Fig. 12. Velocity and temperature fields in neon, case 1. Final $T_h = 2500$ K, $P_i = 1.5$ atm. Transient solution with a 5.0 s bottom wall temperature ramp after: (a) 0.6 s ($V_{max} = 0.004$ m/s), (b) 0.8 s ($V_{max} = 0.01$ m/s), (c) 1.1 s ($V_{max} = 0.1$ m/s), (d) 1.3 s ($V_{max} = 0.2$ m/s), (e) 10.0 s ($V_{max} = 0.2$ m/s); (f) steady-state solution ($V_{max} = 0.2$ m/s).

$$P_f = \frac{nRT}{V} \tag{26}$$

The number of moles of gas in the system can be determined from the initial conditions, and the arithmetic mean of the hot- and cold-wall temperatures in the system, as given in Eq. (20), can be used to evaluate gas properties. Table 2 shows the final system pressure calculated from Eq. (26), the pressure predicted by FLUENT at 10 s, and the percent differences between the two, determined by the equation:

$$\%\text{difference} = \left(\frac{P_{f,\text{FLUENT}} - P_{f,\text{ideal\_gas\_law}}}{P_{f,\text{ideal\_gas\_law}}}\right) \times 100 \tag{27}$$

The largest difference observed is less than 15%, a relatively close agreement.

The pressure rise with time for various bottom-wall temperature ramp rates is shown in Figs. 6 and 7. A change in the slope of the curve is a good indicator of a change in the flow field. This is most clearly illustrated in Fig. 7b for case 2, with an initial pressure of 1.5 atm and a bottom-wall temperature ramp rate of 5.0 s. At around the 5 s mark,

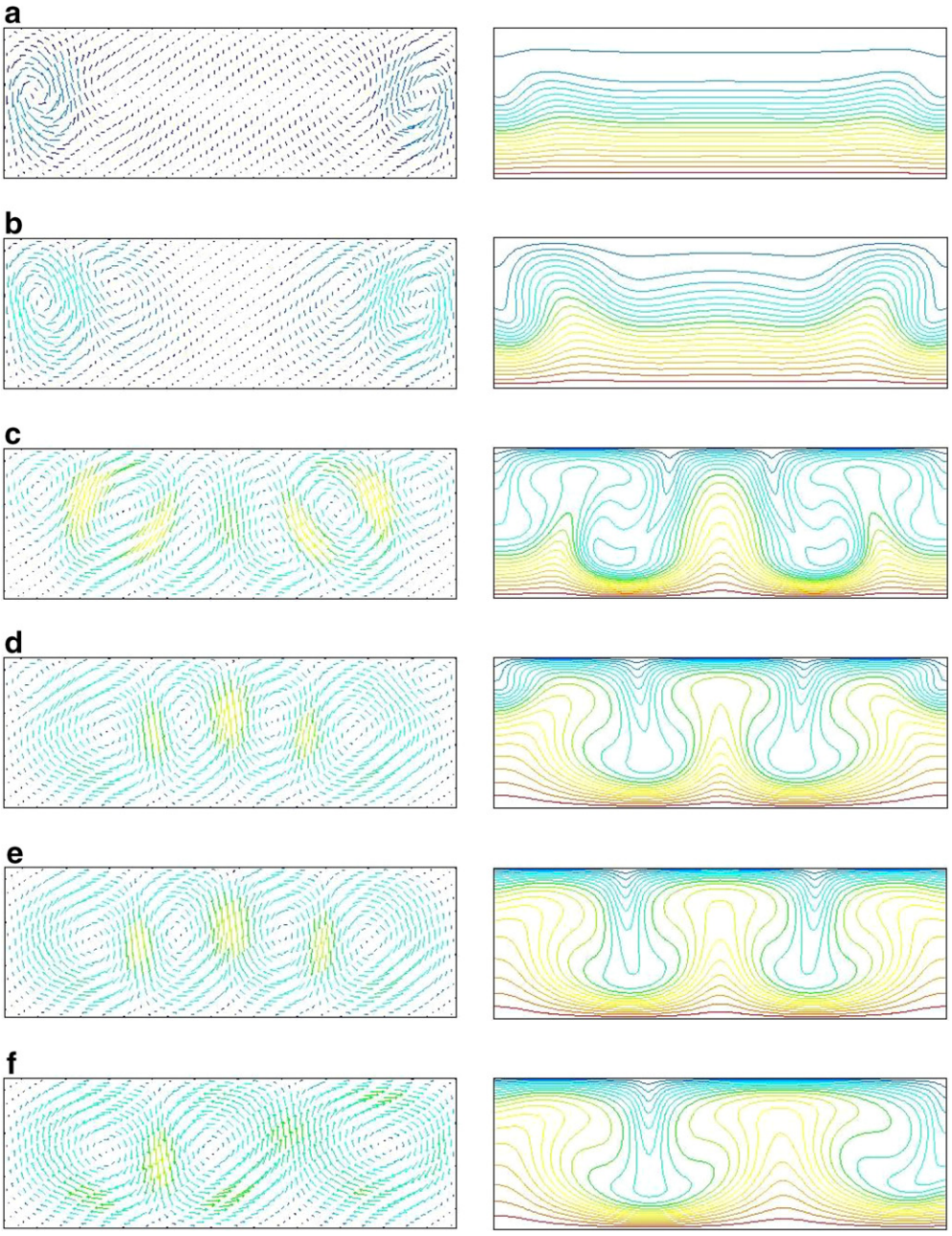

Fig. 13. Velocity and temperature fields in neon, case 2. Final $T_h = 2500$ K, $P_i = 1.0$ atm. Transient solution with a 0.1 s bottom wall temperature ramp after: (a) 0.2 s ($V_{max} = 0.06$ m/s), (b) 0.3 s ($V_{max} = 0.2$ m/s), (c) 0.5 s ($V_{max} = 0.3$ m/s), (d) 0.8 s ($V_{max} = 0.3$ m/s), (e) 10.0 s ($V_{max} = 0.3$ m/s); (f) steady-state solution ($V_{max} = 0.3$ m/s). 0.5 s temperature ramp yields similar results.

the pressure curve changes from a steady rise to a brief plateau. Fig. 8a shows this region in more detail with higher resolution. During about a 0.6-s interval where the pressure drops, Fig. 8b–e shows the transition in the velocity field from six convective cells down to four. An accompanying change in heat transfer rates and temperature in the enclosure causes the observed change in the pressure curve. This observation can be a convenient experimental tool for diagnosing the expected changes in flow behavior in such systems.

Regarding case 1, it was shown in Fig. 4(a) that the pressure vs. hot-wall temperature curves end up in the stable region near the transition between unstable and stable flow for all hot-wall temperature ramp times investigated. This stability map was obtained using steady-state calculations. Fig. 9 shows that when a transient solution is obtained, convective rolls are predicted to be present in the system for the 0.1 and 0.5 s. ramp times. However, the velocity is at such low values at selected times during the transient run that the temperature fields are not significantly affected. This is in contrast to the results obtained from a transient solution shown in Fig. 10. Convective rolls are predicted to be present at a sufficient strength to affect the temperature fields. In both figures, the transient

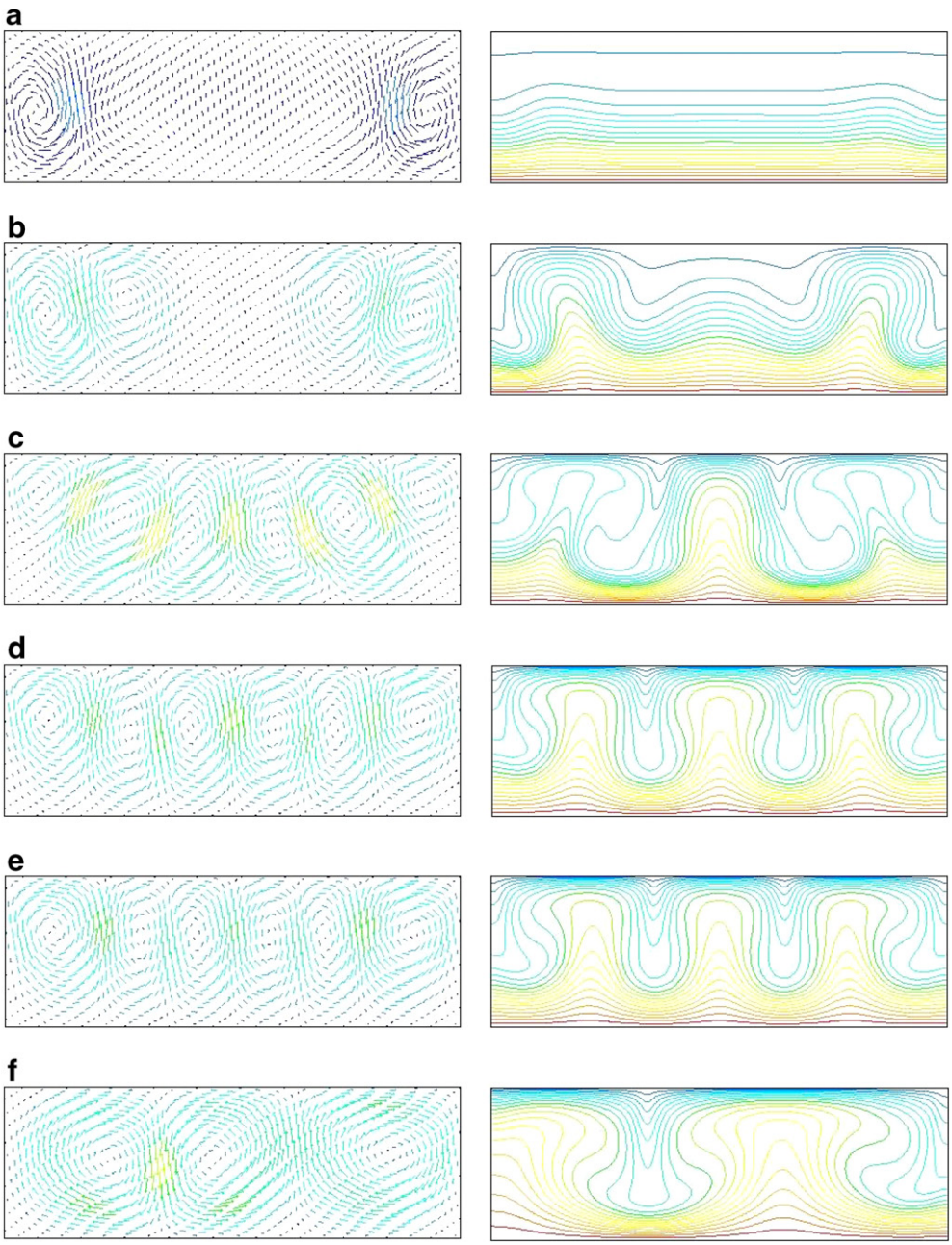

Fig. 14. Velocity and temperature fields in neon, case 2. Final $T_h = 2500$ K, $P_i = 1.0$ atm. Transient solution with a 1.0 s bottom wall temperature ramp after: (a) 0.4 s ($V_{max} = 0.03$ m/s), (b) 0.6 s ($V_{max} = 0.2$ m/s), (c) 0.8 s ($V_{max} = 0.3$ m/s), (d) 3.0 s ($V_{max} = 0.3$ m/s), (e) 10.0 s ($V_{max} = 0.3$ m/s); (f) steady-state solution ($V_{max} = 0.3$ m/s).

solution is seen to no longer be changing at 10 s, indicating that a steady state has been reached. It can be seen that the transient results at ten seconds are different than those predicted by the steady-state solution, pointing out that a transient solution may be necessary to accurately predict the final state of a system such as this. Figs. 11 and 12 show similar results between the steady-state analysis and the transient calculations carried out to ten seconds. Compared to the cases with an initial pressure of 1 atm, these cases with the initial pressure of 1.5 atm show a much greater effect on the temperature field from the velocity field.

Regarding case 2, Figs. 13–15 show that the greater height in case 2 has led to higher velocities compared to case 1, with a corresponding effect in the temperature field. Similar results for an initial pressure of 1.5 atm are shown in Figs. 16–18. At an initial pressure of 1 atm, the number and/or size of the predicted convective rolls is different between the steady-state solution and the transient solution taken out to 10 s. For the cases with an initial pressure of 1.5 atm, on the other hand, steady-state calculations can sometimes predict the final state of the system consistently with the transient calculations. Such discrepancies between steady-state and transient calculations points out again

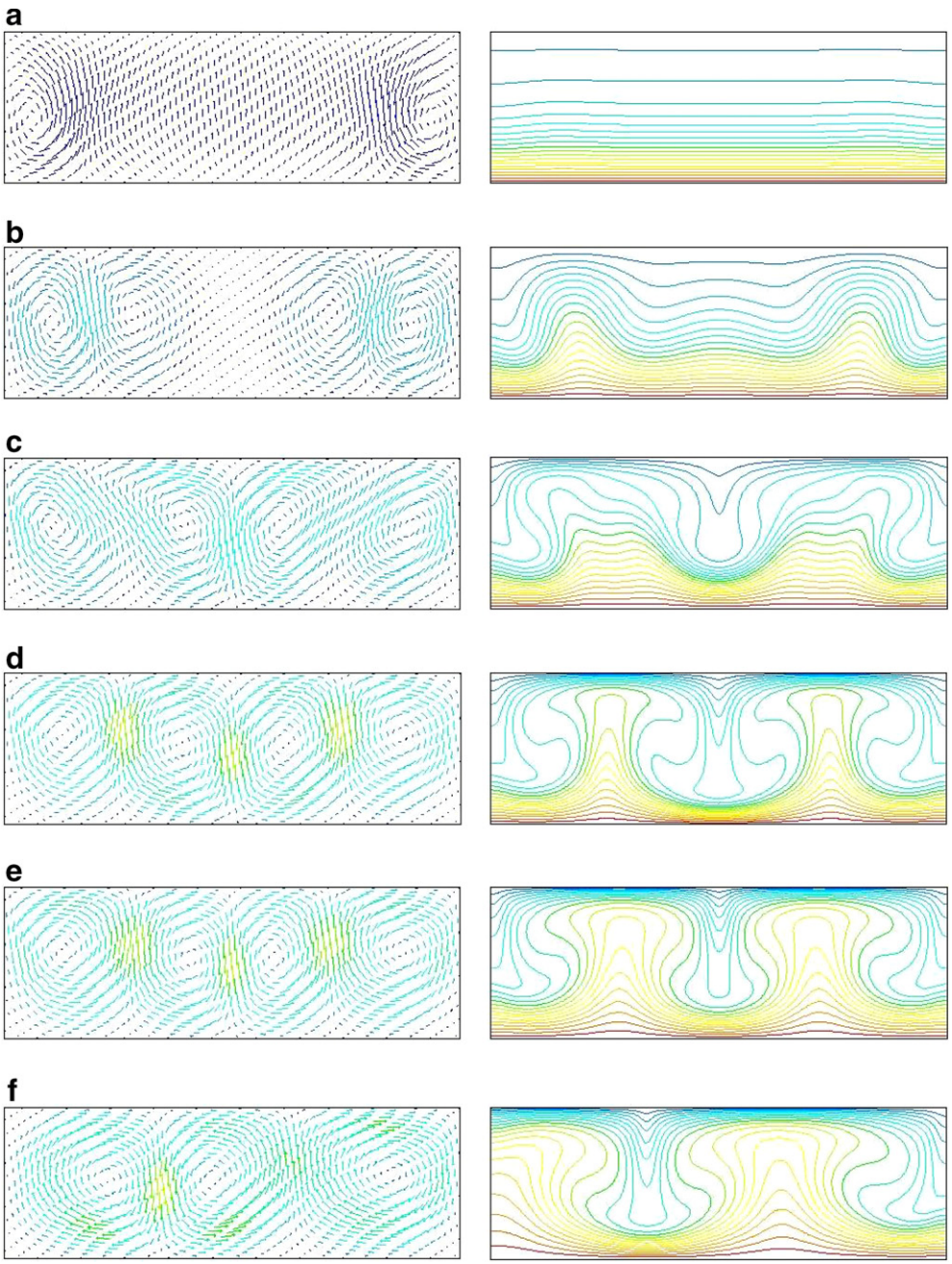

Fig. 15. Velocity and temperature fields in neon, case 2. Final $T_h = 2500$ K, $P_i = 1.0$ atm. Transient solution with a 5.0 s bottom wall temperature ramp after: (a) 0.6 s ($V_{max} = 0.006$ m/s), (b) 1.0 s ($V_{max} = 0.1$ m/s), (c) 1.5 s ($V_{max} = 0.2$ m/s), (d) 2.0 s ($V_{max} = 0.3$ m/s), (e) 10.0 s ($V_{max} = 0.3$ m/s); (f) steady-state solution ($V_{max} = 0.3$ m/s).

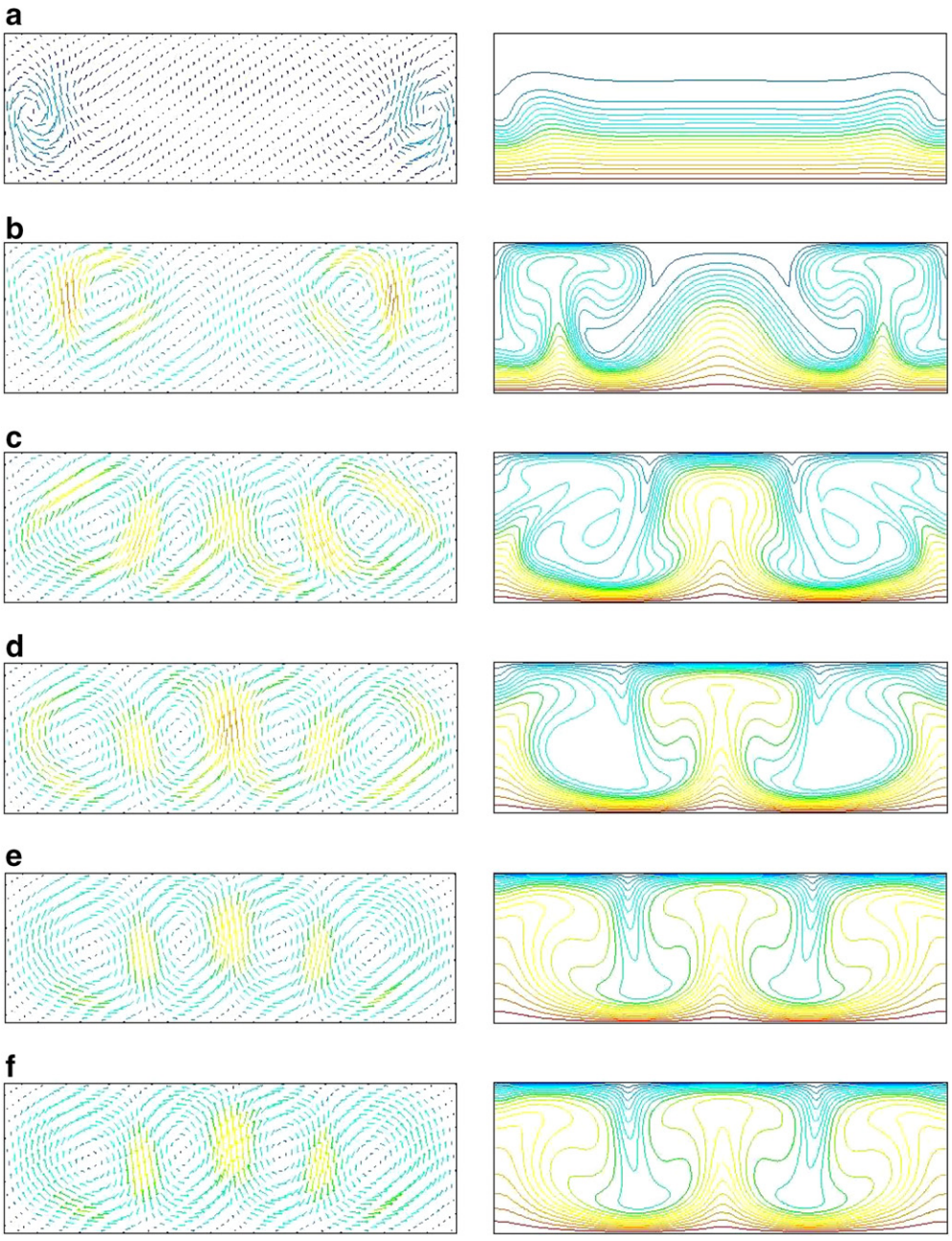

Fig. 16. Velocity and temperature fields in neon, case 2. Final $T_h = 2500$ K, $P_i = 1.5$ atm. Transient solution with a 0.1 s bottom wall temperature ramp after: (a) 0.2 s ($V_{max} = 0.07$ m/s), (b) 0.4 s ($V_{max} = 0.5$ m/s), (c) 0.5 s ($V_{max} = 0.4$ m/s), (d) 0.6 s ($V_{max} = 0.4$ m/s), (e) 10.0 s ($V_{max} = 0.4$ m/s); (f) steady-state solution ($V_{max} = 0.4$ m/s). 0.5 s temperature ramp yields similar results.

that the history of the development of flow structures and their corresponding temperature fields have a profound effect on the eventual final state which can not be properly captured by only steady-state calculations.

Engineering application of existing heat transfer correlations using the Rayleigh and Grashof numbers are common even under conditions where the Boussinesq approximation is not applicable. While this is generally not a problem for liquid systems, this work demonstrates that this will not always be the case for gaseous systems, particularly if hot-wall temperatures exceed about 500 K. Fig. 1 predicts that buoyant convection will tend to be suppressed at higher temperatures. Traditional methods used to calculate the relevant Rayleigh and Grashof numbers for temperatures much beyond 500 K may lead one to conclude that the system is quiescent and conduction-dominated, when it may become unstable and convection-dominated as it is heated to higher temperatures. Even if the convection-dominated regime is predicted, the intensity of the buoyant convection may be misjudged by not considering the history of the system as it is being heated. The consequences of such misjudgments can be severe in

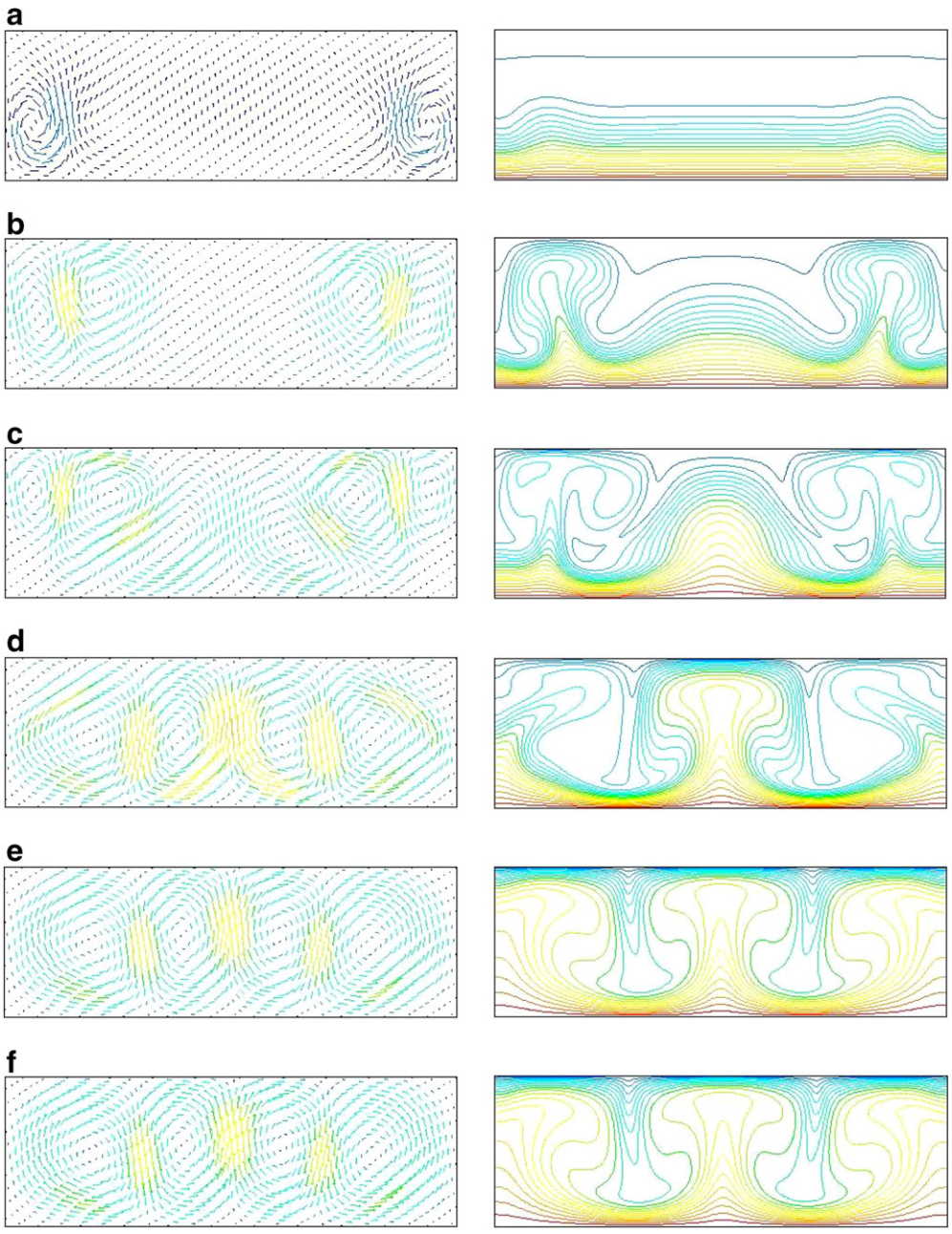

Fig. 17. Velocity and temperature fields in neon, case 2. Final $T_h = 2500$ K, $P_i = 1.5$ atm. Transient solution with a 1.0 s bottom wall temperature ramp after: (a) 0.4 s ($V_{max} = 0.04$ m/s), (b) 0.6 s ($V_{max} = 0.4$ m/s), (c) 0.7 s ($V_{max} = 0.3$ m/s), (d) 0.8 s ($V_{max} = 0.4$ m/s), (e) 10.0 s ($V_{max} = 0.4$ m/s); (f) steady-state solution ($V_{max} = 0.4$ m/s).

applications with partial levels of gravitational acceleration, such as those on the Moon and Mars.

In materials processing involving gaseous media, such as chemical vapor deposition (CVD), deposition uniformity and quality can be improved by avoiding buoyancy-driven convection. The effect of temperature-dependent gas properties on the flow dynamics in CVD processes has long been recognized (Rosenberger, 1987). For example, in horizontal CVD reactors, buoyancy leads to a helical flow structure; in vertical, impinging-jet, or stagnation-flow CVD reactors, buoyancy is suppressed by either enhanced reactant flow rates or by lowering the pressure (Gokoglu, 1992). However, both these approaches lower the efficiency of the process. It has generally been perceived that as the temperature of the hot-wall in CVD increases, buoyant convection will also increase. However, this paper suggests that heating to even higher temperatures may suppress buoyancy. It would be necessary to heat the substrate to these high temperatures rapidly enough to prevent the development of buoyant convection at lower temperatures, but this should be possible with rapid thermal processing (RTP) of materials. It should be noted that the

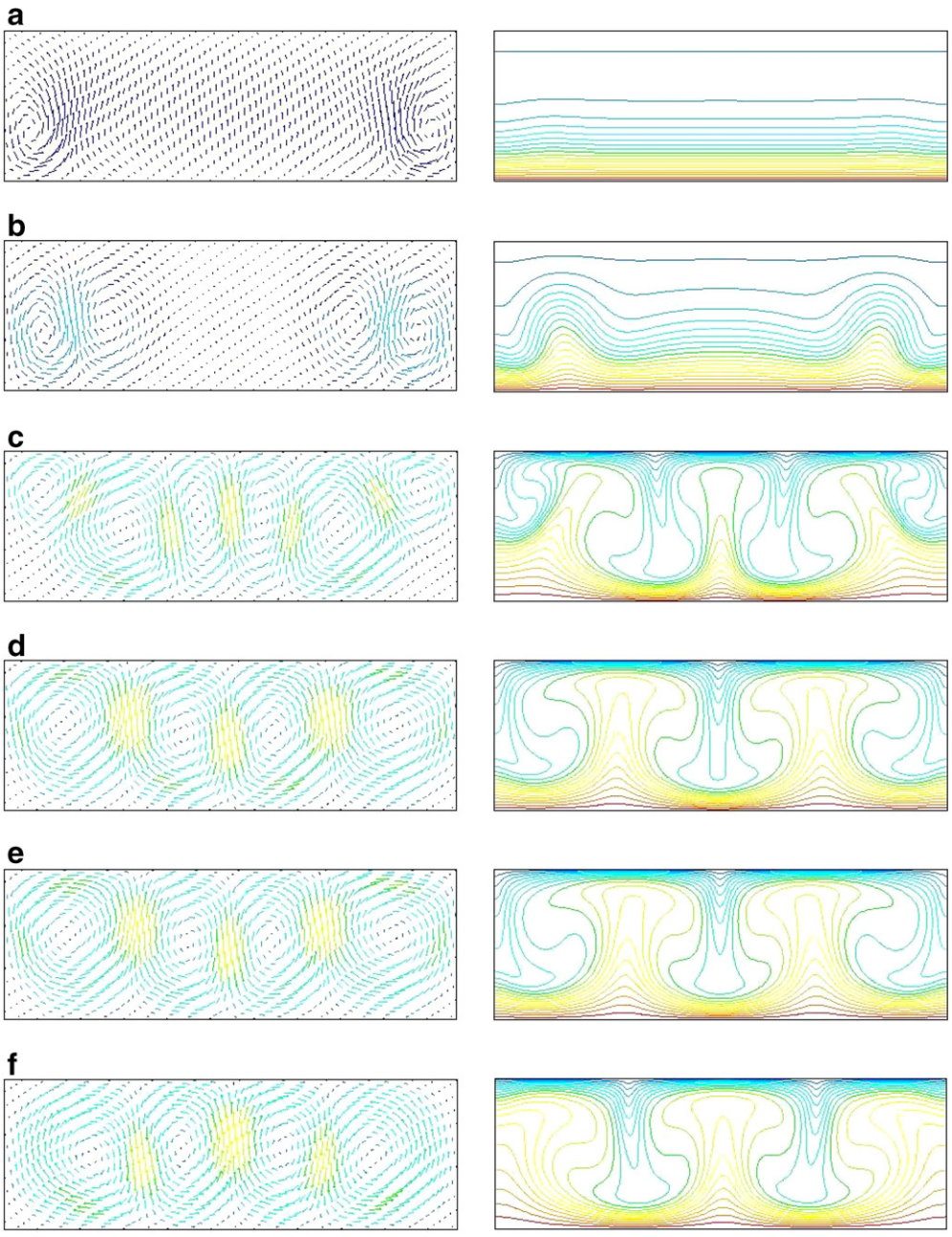

Fig. 18. Velocity and temperature fields in neon, case 2. Final $T_h = 2500$ K, $P_i = 1.5$ atm. Transient solution with a 5.0 s bottom wall temperature ramp after: (a) 0.6 s ($V_{max} = 0.008$ m/s), (b) 0.9 s ($V_{max} = 0.09$ m/s), (c) 3.0 s ($V_{max} = 0.3$ m/s), (d) 6.0 s ($V_{max} = 0.3$ m/s), (e) 10.0 s ($V_{max} = 0.3$ m/s); (f) steady-state solution ($V_{max} = 0.3$ m/s).

low-temperature CVD processes used if high temperatures are harmful to the desired deposit quality can actually increase the likelihood of buoyant convection problems.

The results of this work are directly applicable to partial-gravity combustion applications. Diffusive-transport-controlled flames with planar symmetry create environments with large normalized temperature differences where the traditional application of Rayleigh–Bénard criterion for the onset of convective instability is inadequate (Baumstein and Fendell, 1998; Fendell and Mitchell, 1996). Under non-Boussinesq conditions, it may be necessary to regard the critical Rayleigh number as a function of the Prandtl and Lewis numbers, as well as the normalized temperature difference between the diffusion flame and the cold upper wall. In this type of situation, the thermodynamic dependence of the transport properties becomes a matter of importance.

Applying traditional scaling approaches to micro-scale combustion through the use of dimensionless numbers has proved to be difficult (Sitzki et al., 2001). The critical dimensions of micro-combustors and the heat loss mechanisms for optimal operation require careful analysis. The

results presented here suggest selection of operation temperatures and dimensions between hot- and cold-walls could be done more judiciously to better control conduction- versus convection-dominated heat transfer.

In cryogenic systems, where the "hot" wall may be at room temperature and cryogenically cooled sensors or electronic components may constitute the cold wall, Fig. 1 suggests that the behavior of gaseous systems is quite different for the onset of convective instability. This is because variable gas properties seem to dominate the flow behavior. As shown by the curve labeled $T_c = 50$ K, the system is drastically dampened by the higher gas viscosity when the hot-wall temperature is only 300 K. Heat transfer mechanisms may be quite different than those expected from simpler, Boussinesq-type analyses. If conduction-dominated heat transfer is desired, designers of such systems could benefit from the results presented in this paper by utilizing larger temperature differences.

4. Conclusions

This study demonstrated a capability to define the range of instability in a gaseous enclosed system depending on its geometry, temperature, and pressure. Transient calculations showed that despite ramping the bottom-wall temperature fast enough to minimize the time spent in the unstable region of fluid motion, the final state of the system depends on the final pressure eventually attained after steady state has been reached. The results also showed that steady-state and transient solutions can give different results as to the final state of the system, indicating that the history of the development of flow instabilities is important and that steady-state calculations cannot always be relied upon. Finally, it was demonstrated that changes in the monotonic behavior of the pressure versus time curve in a transient treatment of the problem is a good indicator of changes in flow patterns in the system and can also be used as an experimental diagnostic tool.

Many applications involving heat transfer in gaseous media, such as chemical vapor deposition, combustion, and cryogenics, require knowledge of the onset of convective instability in order to design systems to perform as needed. This work has shown that high temperatures can be effectively used to actually *suppress* buoyant convection in gaseous systems utilizing the enhanced dampening effect of increased gas viscosities. Using existing heat transfer correlations involving the Rayleigh and Grashof numbers under conditions where the Boussinesq approximation is no longer valid (a common practice) could be seriously misleading since the system stability cannot correctly be predicted by these dimensionless numbers. In addition, the intensity of the buoyant convection can be misjudged by not considering the history of the system during heating. Depending on the system conditions, the temperature dependent properties of the gas must be included to fully understand the heat transfer occurring in the system.

Acknowledgement

This work was supported by the Microgravity Combustion Science Program in the Office of Biological and Physical Research at NASA.

References

Baumstein, A., Fendell, F., 1998. Strain-rate-free diffusion flames: initiation, properties, and quenching. Combust. Sci. Technol. 132, 157–198.

Bird, R.B., Stewart, W.E., Lightfoot, E.N., 1960. Transport Phenomena. John Wiley & Sons, New York, NY.

Brown, W.B. Donoughe, P.L., 1951. Tables of Exact Laminar Boundary Layer Solutions When the Wall is Porous and Fluid Properties are Variable. NACA TN 2479.

Caretto, L.S., Gosman, A.D., Patankar, S.V., Spalding, D.B., 1972. Two Calculations Procedures for Steady, Three-Dimensional Flows with Recirculation, Proceedings of the Third International Conference on Numerical Methods in Fluid Dynamics. Springer-Verlag, pp. 60–68.

Fendell, F.E., Mitchell, J.A., 1996. Feasibility of planar, unidirectional-flow diffusion flames in earth gravity. Combust. Sci. Technol. 120, 83–117.

Ferzieger, J.L., Peric, M., 1996. Computational Methods for Fluid Dynamics. Springer-Verlag, Heidelberg.

FLUENT, Fluent, Inc., Lebanon, New Hampshire.

Fluent, Inc., 2005. FLUENT User's Guide. Fluent, Inc., Lebanon, New Hampshire.

Frolich, J., Laure, P., Peyret, R., 1992. Large departures from Boussinesq approximation in the Rayleigh–Bénard Problem. Phys. Fluids A 4 (7), 1355–1372.

Gokoglu, S.A. 1992. Chemical vapor deposition modeling for high-temperature materials, chemical vapor deposition of refractory metals and ceramics II, Eds. Besmann, T.M., Gallois, B.M., Warren J.W., Mater. Res. Soc. Symp. Proc., 250, 17–28.

Gokoglu, S.A., Kuczmarski, M.A., 2003. Suppression of buoyancy in gaseous media at high temperatures. In: Proceedings of the Fourth International Symposium on Scale Modeling, Cleveland, Ohio, USA, 2003, pp. 74–84.

Goldstein, R.J., Volino, R.J., 1995. Onset and development of natural convection above a suddenly heated horizontal surface. J. Heat Transfer 117, 808–821.

Gray, D.D., Giorgini, 1976. The validity of the Boussinesq approximation for liquids and gases. Int. J. Heat Mass Transfer 19, 545–551.

Hirschfelder, J.P., Curitss, C.F., Bird, R.B., 1954. Molecular Theory of Gases and Liquids. J. Wiley and Sons, New York.

Issa, R.I., 1986. Solution of implicitly discretized fluid flow equations by operator splitting. J. Comput. Phys. 62, 40–65.

Kays, W.M., Crawford, M.E., 1980. Convective Heat and Mass Transfer, second ed. McGraw-Hill, New York, NY.

Kennard, E.M., 1938. Kinetic Theory of Gases. McGraw Hill, New York.

Paolucci, S., Chenoweth, D.R., 1987. Departures from the Boussinesq approximation in laminar Bénard convection. Phys. Fluids 30 (5), 1561–1564.

Patankar, S.V., 1980. Numerical Heat Transfer and Fluid Flow. McGraw-Hill, New York, NY.

Rosenberger, F., 1987. Flow dynamics and modelling of CVD. In: Cullen, G.W. (Ed.), Proceedings of the Tenth International Conference on Chemical Vapor Deposition. The Electrochemical Soc., Pennington, NJ, pp. 11–22.

Sitzki, L., Borer, K., Schuster, E., Ronney, P.D., Wussow, S. 2001. Combustion in micro-scale heat-recirculating burners. In: Third Asia-Pacific Conference on Combustion, Seoul, Korea.

Svehla, R.A., 1962. Estimated viscosities and thermal conductivities of gases at high temperatures. NASA Technical Report-132.